3-D Inversion of Gravity Anomalies by Combining Power-Spectrum Derived Adaptive Weighting and Cross-Gradient Regulation: Application to Molybdenum–Copper Deposit

Guoqing Ma, Tingyi Wang, Qingfa Meng, Zongrui Li, Taihan Wang, and Lili Li

***Abstract*— Gravity measurement is an important geophysical prospecting method for mineral exploration. With most of the shallow ore deposits in China being exploited, the future targets for exploration will be aimed at the deep mineral resources about 4-km underground. To improve the resolving ability in the vertical direction of the 3-D density inversion to find deep-source minerals, we propose to achieve the inversion of gravity anomalies by combining power-spectrum derived adaptive weighting and cross-gradient regularization. First, spectral analysis is utilized to conduct the source-depth separation, and the adaptive weighting function is designed depending on the slope of the radial logarithmic power spectrum of the gravity anomaly, which can enhance the correspondence for the field sources with different depths to improve the vertical resolution relatively. Thus, each separated source with different depths could be given an adaptive weighting coefficient in each separated inversion. Second, the cross-gradient technique is introduced as a structural constraint in the objective function to further constrain the separated inversion process. By performing two-cuboid-source cases, it can be seen that this combination calculated approach has great potential to improve the quality of the inversion results. When examining the inversion of the actual gravity data from certain ore district in the west of Zhen'an, South Qinling, we speculate that a potential deep ore body would exist in the deposit via utilizing the recovered density model obtained by the proposed method.**

***Index Terms*— Adaptive weighting function, combination inversion, gravity anomaly, logarithmic power spectrum.**

I. Introduction

THE 3-D density inversion of gravity anomalies is a common method to quantitatively calculate the physical parameters of the underground geological body [1]–[4]. However, the inversion problem is commonly ill-posed, which would cause the inherent nonuniqueness of the results [5]. One of the ways to obtain more accurate results is to add prior information. Sufficient prior information, either from well logs, other geophysical exploration, or geological data, would be useful to solve the problem. However, the external information is hard to be obtained because it is difficult to investigate and explore in certain areas, such as in the desert and forest. Another available method to add prior information is to introduce a reference model.

Last and Kubik [6] developed a compact inversion method by adding a constraint to minimize the structural volume of abnormal bodies in the iterative inversion process. This approach is applicable to simulate gravity anomaly with single-density sources and has good recognition ability for the shallow geological body as well. Guillen and Menichetti [7] searched for solutions minimizing the moment of inertia in the inversion process. The results of the inversion are both deeper and more compact. After that, Barbosa and Silva [8] modified this constraint by incorporating prior information about the maximum compactness of the anomalous sources along several axes. It provides versatility dealing with more complex gravity inversion problems. The depth weighting function was introduced into the objective function of inversion, which effectively reduced the skin effect to improve the vertical resolution [9]. Portniaguine and Zhdanov [10] introduced the gradient minimum as a constraint, and the focusing inversion method was proposed to make the inversion results more concentrated and the boundary of the anomaly body more distinct. A cokriging inversion method was applied to geophysical data inversion [11], in which the information of the rock dip direction and dip angle can be easily added [12]. Vatankhah *et al.* [13] used the minimum support stabilizer to determine the optimal regularization parameters in the context of the 3-D focusing gravity inversion method improving the accuracy of the inversion results. Ghalehnoee and Ansari [14] added the kernel function matrix as the weighting function in the inversion process to balance the influence of the nonuniformity of the kernel function on the calculation process. Another approach based on marginalizing the probabilistic inversion method was presented, in which the inverse domain is partitioned into various zones and each domain could have its own covariance matrix [15]. Li *et al.* [16] developed a 3-D sparse inversion method for gravity, which made more effective use of the known physical property information to improve the resolution of the inversion results.

Manuscript received September 13, 2021; revised November 19, 2021 and February 16, 2022; accepted March 22, 2022. Date of publication March 28, 2022; date of current version April 15, 2022. This work was supported by the National Natural Science Foundation of China under Grant 42074147. *(Corresponding author: Qingfa Meng.)*

The authors are with the College of Geo-Exploration Sciences and Technology and the Institute of National Development and Security Studies, Jilin University, Changchun 130026, China (e-mail: maguoqing@jlu.edu.cn; wang.tingyi@foxmail.com; mengqf19@mails.jlu.edu.cn; 2199327023@qq.com; wangtaihan@jlu.edu.cn; lilili@jlu.edu.cn).

Digital Object Identifier 10.1109/TGRS.2022.3162638

Obviously, different algorithms are designed according to the available measured data, prior information, and the studied area. It is well known that the gravity anomaly is a comprehensive reflection of the density variation below the observation surface (e.g., [17]–[19]), Bhattacharyya and Leu [20] utilized the slope of the power spectral density as a means of source depth to distinguish sources with different depths. Though the assumptions underlying it is questioned, the method that minimizing the misfit between the model and the observed power spectrum yields an estimate for the depth to the top of the sources is still recognized [21]. Thus, spectral analysis is accepted and practical to derive the source-depth separation [22].

In this article, the 3-D inversion method by combining power-spectrum derived adaptive weighting and cross-gradient regularization is proposed. First, the anomalies with different burial depths from the comprehensive anomaly are separated, and the separated anomalies are given matched weighting functions based on the logarithmic power spectrum. Next, the constraint of the cross gradient is utilized to derive the combination inversion result. The proposed method is applied to the synthetic data, and the minimum norm inversion method is applied to the same data for comparison. The inversion of the real gravity data from South Qinling also yields a density reconstruction result for obtaining the location of potential ore bodies.

II. Methodology

For the density inversion of gravity data, the subsurface is divided into prismatic cells, and the density change of each cell can be computed. The relationship between density ρ and anomaly g can be expressed as

$$G\rho = g \tag{1}$$

where ρ is the residual density of each discrete unit, g is the observation gravity anomaly, and G is the kernel function matrix.

The inversion problem is commonly converted to the issue of solving the optimal solution of the objective function, and the objective function of the minimum norm inversion method can be commonly written as [23]

$$\varphi(\rho) = \|W_d(G\rho - g)\|_2^2 + \alpha\|W_\rho \rho\|_2^2 \tag{2}$$

where W_d is the data weighting matrix, α is the regularization parameter, and the depth weighting function is

$$W_\rho = (z + z_0)^{-\beta/2} \tag{3}$$

where z_0 depends on the cell size of the model discretization and the observation height of the data and β is the weighting coefficient. Li and Oldenburg [9], [24] suggested that $\beta = 2$ in the gravity case and $\beta = 3$ in the magnetic case, respectively. This means that once the parameter β is fixed, the weighting function would be consistent.

The gravity anomaly is a comprehensive reflection of the underground density change [25], and thus, the density inversion method, using a uniform depth weighting function for the superimposed gravity anomaly, is not an appropriate strategy to obtain the precise distribution of the sources with different depths; it cannot meet the requirement for the realistic source distribution. Hence, we propose a 3-D inversion method by combining power-spectrum derived adaptive weighting and cross-gradient regularization.

To introduce the proposed method, the principle that the slope of the logarithmic power spectrum can reflect the sources with different depths should be known as a premise. First, to fix the problem of the consistent weighting function, we design an adaptive weighting function and the anomalies with different depths from the superimposed anomaly are separated, according to the slope variation of the logarithmic power spectrum. The correlation expression between the logarithmic power spectrum and the buried depth of the source is

$$\ln\ P = \ln\ l - 2hr \tag{4}$$

where $P = le^{-rh}$ is the power spectrum function at any depth h, l is the factor related to the physical parameters of the geological body, and $r = (u^2 + v^2)^{1/2}$ is the radial circular frequency, in which u and v are the wavenumbers in the x- and y-directions, respectively.

Due to the fact that the slope of the logarithmic power spectrum approximates to the source depth, we express the calculation of the adaptive weighting function related to the slope of the logarithmic power spectrum, which is written as

$$W_{\rho i} = (z + z_0)^{-(k/k_i + 1/\beta)} \tag{5}$$

where k is the linear fitting line's slope of power-spectrum curve, k_i is the linear fitting line's slope of the ith segment of the power-spectrum curve, and $\beta = 2$ as suggested in [9].

The Butterworth filter is used to separate anomalies with different depths on the inflection point of the power-spectrum curve [26], and the expression of the Butterworth filter is written as [27]

$$H_n(r, w) = [1 + (r/w)^{2n}]^{-1/2} \tag{6}$$

where n is the filter order and w is the truncated wavenumber, which can be derived by the inflection point of radial logarithmic power-spectrum curve.

Thus, the anomaly can be separated into multiple components by the filter, according to the logarithmic power spectrum

$$\begin{cases} \tilde{g}_i = \left[\tilde{g} - \sum_{j=1}^{i-1} \tilde{g}_j\right] \cdot H_n(r, w) \\ \tilde{g}_N = \tilde{g} - \sum_{j=1}^{N-1} \tilde{g}_j \end{cases} \tag{7}$$

where $\tilde{g}_i$ is the ith frequency spectrum.

The anomalies obtained after the separation are not completely unrelated, so we adopt the cross gradient as a mutual structural constraint to realize the inversion of the separated anomalies [28], [29], and the objective function corresponding to the ith separated anomaly is

$$\Phi_i = \|W_{di}(G\rho_i - g_i)\|_2^2 + \alpha_i\|W_{\rho i}\rho_i\|_2^2 + \sum_{\substack{j=1 \\ j\neq i}}^{n} \lambda_{i,j}\Phi_{\text{cross}}(\rho_i, \rho_j) \tag{8}$$

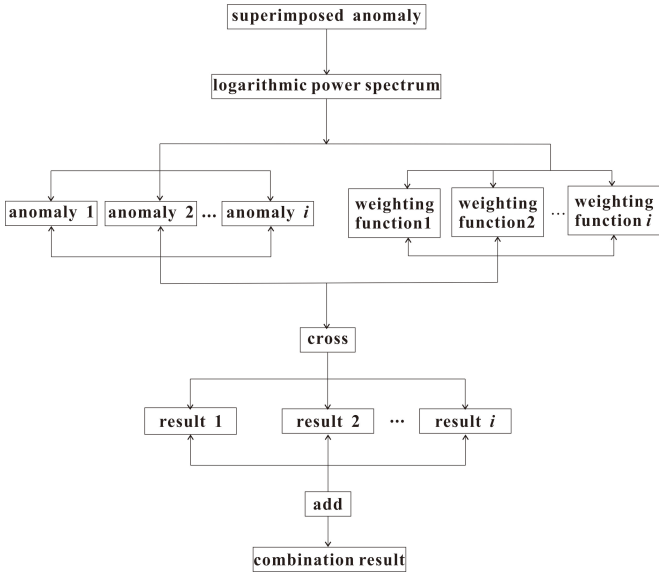

Fig. 1. Flowchart of the proposed inversion algorithm.

where $\Phi_{\text{cross}}(\rho_i, \rho_j) = \nabla\rho_i \times \nabla\rho_j$ is the cross-gradient operator [30], W_{di} is the data weighting matrix, α_i is the regularization parameter, $\lambda_{i,j}$ is the coefficient of the cross-gradient operator, and W_{pi} is the adaptive depth weighting function, which is related to the slope of the logarithmic power spectrum. In this article, the L-curve method is used to adjust the regularization parameters and cross-gradient operator to achieve the balance between data fitting and model constraints in the objective function [31].

After that, the conjugate gradient algorithm is used to solve the optimal solutions of the objective functions [32], and each inversion result of n anomalies is directly added to obtain the final inversion result

$$\rho = \rho_1 + \rho_2 + \cdots + \rho_n. \tag{9}$$

In all inversions, the formula

$$E = \sqrt{\sum_{i=1}^{N} \|G\rho_i - g_i\|_2^2 / M} \tag{10}$$

is used to calculate the misfit error, and when it is less than 0.01 mGal, the calculation can be stopped; we consider that the results can be trusted.

The combination result can be obtained through the calculation flowchart, as shown in Fig. 1. In this algorithm, we first calculate the logarithmic power spectrum of the superimposed anomaly, and the anomalies with different depths can be separated from the superimposed anomaly. The second step is to invert each anomaly separately with an adaptive weighting function constrained by the cross-gradient technique, and we use (10) to decide whether the inversion calculation can be stopped. Finally, the combination result can be derived by directly adding each separate result.

III. Model Studies

A single-cuboid-source case is considered to demonstrate the accuracy of the proposed method by model tests.

TABLE I
Model Parameters

Number	Model	Center Coordinates	Extent	Density Contrast
Case 1	Cuboid	(950, 950, 350) m	300 m × 300 m × 300 m	1.0 g/cm^3
Case 2	Deep cuboid	(750, 950, 550) m	700 m × 700 m × 300 m	1.0 g/cm^3
	Shallow cuboid	(1650, 950, 350) m	300 m × 300 m × 300 m	1.0 g/cm^3
Case 3	Deep cuboid	(950, 950, 950) m	700 m × 700 m × 400 m	1.0 g/cm^3
	Shallow cuboid	(950, 950, 350) m	300 m × 300 m × 300 m	1.0 g/cm^3

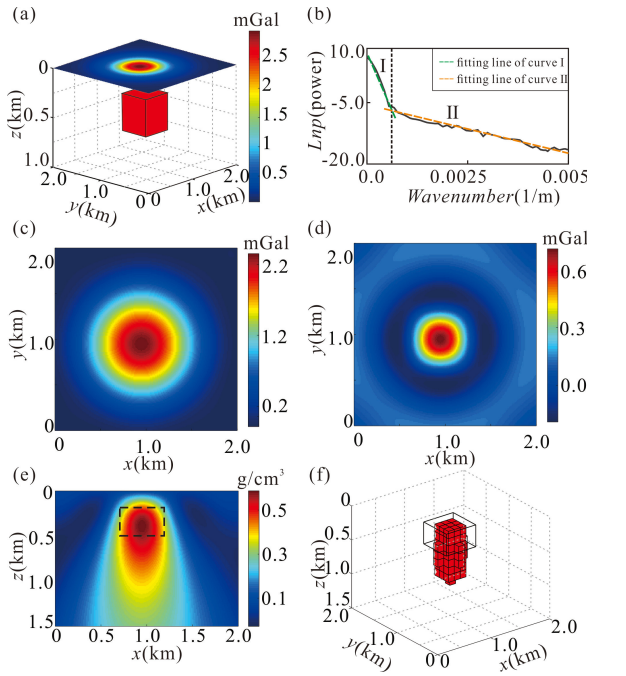

Fig. 2. Single-cuboid-source case. (a) Cuboid position and its gravity anomaly. (b) Power spectrum. (c) Low-frequency anomaly after separation. (d) High-frequency anomaly after separation. (e) Slice at $y = 950$ m of the direct inversion result obtained by the minimum norm inversion method. (f) 3-D perspective view of the inversion result.

The cuboid [Fig. 2(a)] is centered at (950, 950, 350) m with an extent of (500, 500, 300) m whose density contrast is 1.0 g/cm^3 with surrounding rocks, and the parameters of the cuboids used in this article are shown in Table I. The grid step in the x- and y-directions of the data [Fig. 2(a)] is 100 m, and the values are the same in the following model tests. In all inversions, the subsurface is divided into 20 × 20 × 15 prismatic cells and the sampling interval is equal to the horizontal interval of the cells, which could make the inversion results more credible [5].

The logarithmic power spectrum is shown in Fig. 2(b) for the gravity anomaly of the cuboid. It can be seen that the curve has an obvious inflection point so that the curve can be divided into two sections marked as I and II. This means that the

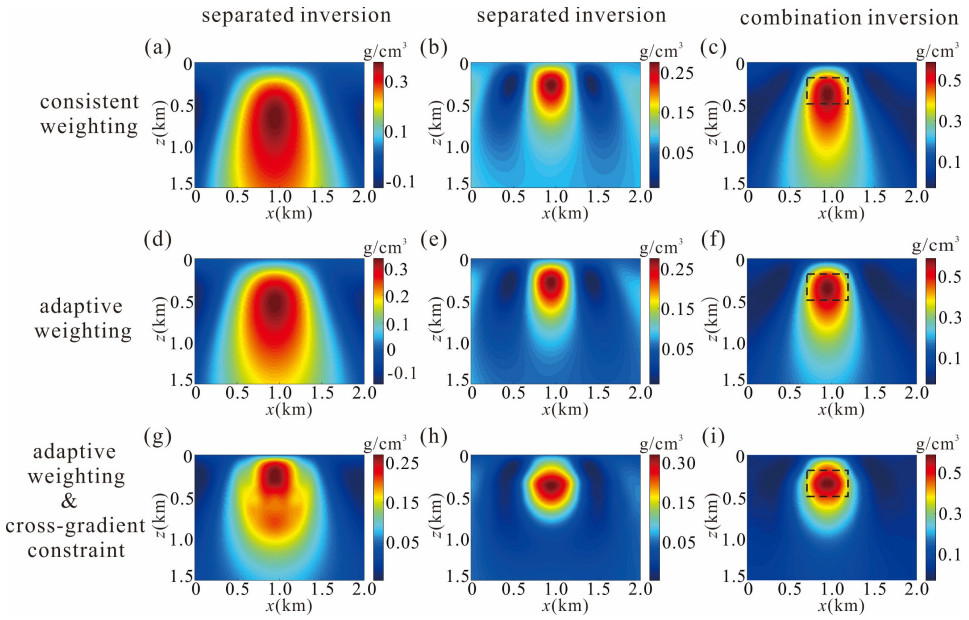

Fig. 3. Slices at $y = 950$ m of the separated and combination inversion results. (a) Slice of the low-frequency anomaly's inversion result obtained by consistent weighting. (b) Slice of the high-frequency anomaly's inversion result obtained by consistent weighting. (c) Slice of combination inversion result obtained by consistent weighting. (d) Slice of the low-frequency anomaly's inversion result obtained by adaptive weighting. (e) Slice of the high-frequency anomaly's inversion result obtained by adaptive weighting. (f) Slice of combination inversion result obtained by adaptive weighting. (g) Slice of the low-frequency anomaly's inversion result obtained by combining adaptive weighting and cross-gradient constraint. (h) Slice of the high-frequency anomaly's inversion result obtained by combining adaptive weighting and cross-gradient constraint. (i) Slice of combination inversion result obtained by combining adaptive weighting and cross-gradient constraint.

anomaly can be divided into two frequency segments, which reflect different depth information. Accordingly, we select the wavenumber corresponding to the inflection point of the curve to divide the field source into two parts with different depth information. As a result, the low-frequency anomaly [Fig. 2(c)] and the high-frequency anomaly [Fig. 2(d)] can be separated from the superimposed anomaly. We directly invert the original anomaly in Fig. 2(a) by the minimum norm inversion method; the slice at $y = 950$ m of the direct inversion result can be obtained [Fig. 2(e)] and the 3-D perspective view with a truncation density of 0.38 g/cm^3 is shown in Fig. 2(f).

Next, we invert the separated anomalies obtained by the same method with the consistent weighting function. The separated inversion result of the low-frequency anomaly with consistent weighting function is shown in Fig. 3(a), and the separated inversion result of the high-frequency anomaly with consistent weighting function is shown in Fig. 3(b). The slice at $y = 950$ m of the combination inversion result [Fig. 3(c)] can be obtained by adding the slices of the two separated inversion results [Fig. 3(a) and (b)] directly. Thus, the final inversion result of the model can be obtained. When we compared this final inversion result with the direct inversion result [Fig. 2(e)], it can be found that the amplitude and center position are almost the same. This result illustrates that the method of adding each inversion result of the separated anomalies is correct.

In addition, we consider an adaptive weighting function related to the power spectrum in the separated inversion calculation according to the different weights that sources occupy in the total field. The slice at $y = 950$ m of the inversion results of the low-frequency anomaly and the high-frequency anomaly is, respectively, shown in Fig. 3(d) and (e), and the

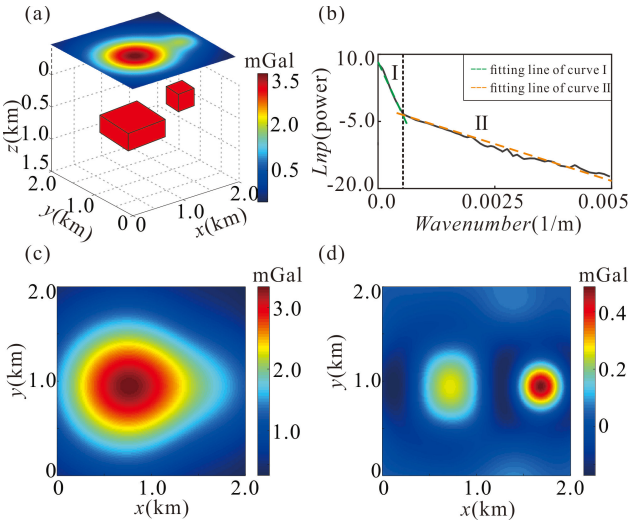

Fig. 4. Two-cuboid-source case. (a) Cuboid position and its gravity anomaly. (b) Logarithmic power spectrum. (c) Low-frequency anomaly after separation. (d) High-frequency anomaly after separation.

combination inversion result is shown in Fig. 3(f). It can be seen that the final inversion result with adaptive weighting is more convergent than the inversion result with consistent weighting, which is shown in Fig. 3(c). Furthermore, we introduce the cross-gradient operator into the separated inversion calculation process and the results are shown in Fig. 3(g) and (h). Each separated anomaly can be constrained in the horizontal direction. It can be found that the spatial resolution of the slice at $y = 950$ m of the combination inversion result in Fig. 3(i) is greatly improved. Thus, the accuracy and superiority of the proposed method can be proved.

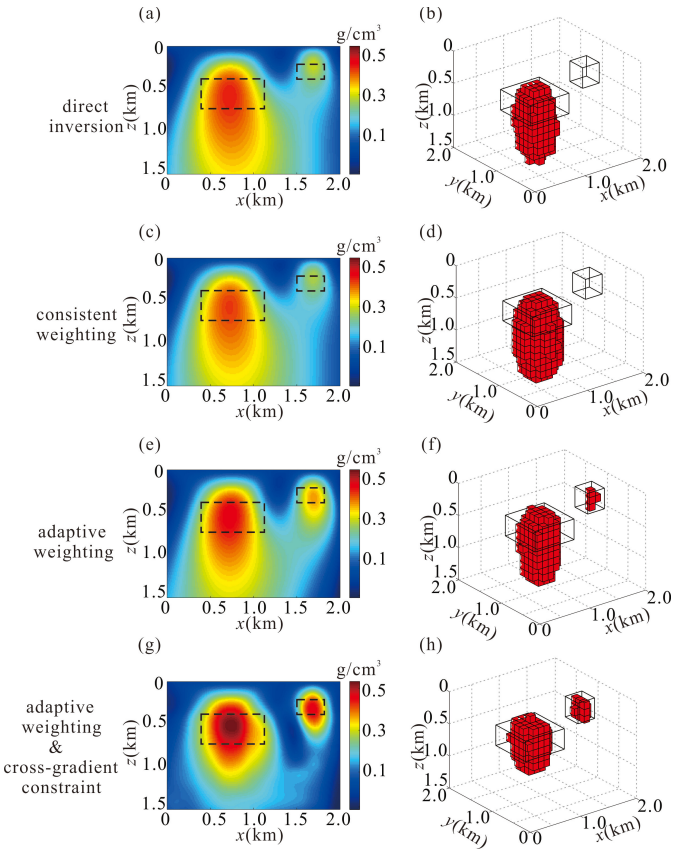

Fig. 5. Slices at $y = 950$ m of the combination inversion results by different methods and their respective 3-D perspective view of the inversion results. (a) Slice of direct inversion result of the original anomaly derived by the minimum norm inversion method. (b) 3-D perspective view of the direct inversion result. (c) Slice of the combination inversion result of the separated anomalies derived by the minimum norm inversion method with consistent weighting. (d) 3-D perspective view of the combination inversion result with consistent weighting. (e) Slice of the combination inversion result of the separated anomalies derived by the minimum norm inversion method with adaptive weighting. (f) 3-D perspective view of the combination inversion result with adaptive weighting. (g) Slice of the combination inversion result of the separated anomalies derived by combining adaptive weighting and cross-gradient constraint. (h) 3-D perspective view of the combination inversion derived by combining adaptive weighting and cross-gradient constraint.

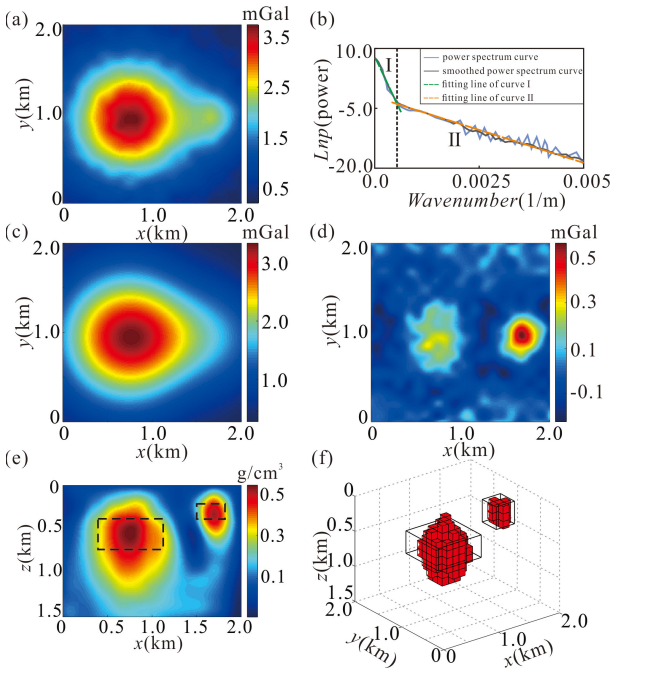

Fig. 6. Antinoise experiment. (a) Gravity anomaly of two-cuboid-source case with 3% Gaussian noise. (b) Logarithmic power spectrum. (c) Low-frequency anomaly after separation. (d) High-frequency anomaly after separation. (e) Slice at $y = 950$ m of the combination inversion result obtained by the proposed method. (f) 3-D perspective view of the combination result.

Next, we set a model [Fig. 4(a)] in which two cuboids have different depths to check the applicability of the method. The center coordinates of the shallow cuboid are (1650, 950, 350) m with an extent of (300, 300, 300) m and the deep cuboid, which contributes as the main field anomalies are located in (750, 950, 550) m with an extent of (700, 700, 300) m. It can be seen that the anomaly produced by the deep source is dominant over the superimposed anomaly and occupies greater weight so that the response of the shallow source is weak. Directly inverting the superimposed anomaly would obscure the result by focusing on the dominant anomaly since it would be difficult to recognize the shallow cuboid from the inversion result.

The logarithmic power spectrum of the anomaly is calculated [Fig. 4(b)], and the low-frequency anomaly [Fig. 4(c)] and the high-frequency anomaly [Fig. 4(d)] can be obtained according to the slope variation of the logarithmic power spectrum. It is obvious that the anomalies generated by the two cuboids can be separated from the superimposed anomaly, and the separated high-frequency anomaly also contains some low-frequency information. However, the high-frequency component still has been relatively highlighted after the separation.

The slice at $y = 950$ m of the direct inversion result of the original anomaly derived by the minimum norm inversion method is shown in Fig. 5(a), and its 3-D perspective view with a truncation density of 0.32 g/cm^3 is shown in Fig. 5(b). Next, the low-frequency anomaly [Fig. 4(c)] and the high-frequency anomaly [Fig. 4(d)] are separately inverted by the minimum norm method with consistent weighting; the slice at $y = 950$ m of the final inversion result [Fig. 5(c)] is obtained and its 3-D perspective view with the same truncation density of 0.32 g/cm^3 is shown in Fig. 5(d). When considering to invert the low-frequency anomaly [Fig. 4(c)] and the high-frequency anomaly [Fig. 4(d)] with adaptive weighting, the slice at $y = 950$ m of the adding inversion result is shown in Fig. 5(e) and its 3-D perspective view is shown in Fig. 5(f). Since the low-frequency anomaly [Fig. 4(c)] and the high-frequency anomaly [Fig. 4(d)] are not completely unrelated, the cross-gradient operator can restrain the homologous part. Introducing the cross-gradient operator in the inversion calculation, the separated anomalies are inverted with adaptive weighting and the combination result [Fig. 5(g)] can be obtained by adding two separated results directly and its 3-D perspective view with the truncation density of 0.32 g/cm^3 is shown in Fig. 5(f). It can be seen that the weak anomaly is better recovered, and the deep cuboid has better convergence from the slice at $y = 950$ m of inversion result obtained by the proposed method when compared with other two methods. When compared with the 3-D perspective views, the result obtained by the minimum norm inversion method with consistent weighting in Fig. 5(d) shows that it cannot recover the location of the shallow cuboid,

and the result of the deep cuboid is extremely divergent so that it is hard to accurately determine the depth of the cuboid in the vertical direction. With the utilization of adaptive weighting, the inversion result [Fig. 5(f)] is improved to some extent. However, the vertical resolution of the inversion result is still poor. Meanwhile, the combination inversion result obtained by the proposed method [Fig. 5(h)] illustrates the location and extent of the shallow cuboid, and the vertical resolution of the deep cuboid is much higher.

To simulate the designed anomaly closer to the actual exploration data, Gaussian noise with a signal-to-noise ratio of 3 is added to the data of the two-cuboid-source case [Fig. 4(a)] and the anomaly with noise is shown in Fig. 6(a). The logarithmic power spectrum of the data with noise is shown in Fig. 6(b), and the curve is hard to be used to do the slope fitting because the curve fluctuates in high-frequency section after adding Gaussian noise. Thus, the five-point-average method [33] is used to process to get the smoothed curve in Fig. 6(b), but the noise and the valid information would still overlap on the curve after smoothing. Next, the superimposed anomaly is separated into a low-frequency anomaly [Fig. 6(c)] and a high-frequency anomaly [Fig. 6(d)] according to the smoothed curve of the power spectrum. Because the noise is characterized by high frequency, the influence of the added noise is mainly concentrated in the high-frequency part after separation, and the separated high-frequency anomaly has some distortions. The anomaly with noise is inverted by the proposed method and the adaptive weighting function is the same as the last experiment. The slice at $y = 950$ m of the final inversion result obtained by the proposed method is shown in Fig. 6(e), and the 3-D perspective view with a truncation density of 0.32 g/cm^3 is shown in Fig. 6(f). When we compared the slice of the inversion result [Fig. 6(e)] with the slice in Fig. 5(g), it can be found that there is little difference between the two results, and the resolution of the 3-D perspective view of the inversion result in Fig. 6(f) has no significant change compared with that in Fig. 5(h), so the added noise has little influence on the inversion result. In other words, adding uncorrelated Gaussian random noise does not impact the results much.

At this point, it is still difficult to find the deep ore body, which is one of the reasons that the response of the shallow ore body covers the deep part, making it impossible to distinguish. To simulate the distribution of this actual underground geological body, we design a two-cuboid-source case in which the central coordinates of the two cuboids are on a vertical line [Fig. 7(a)]. The center coordinates of the shallow cuboid are (950, 950, 350) m with an extent of (300, 300, 300) m and the deep cuboid located in (950, 950, 950) m with an extent of (700, 700, 400) m. We find that it is difficult to distinguish how many field sources exist by observing the anomaly directly. The logarithmic power spectrum of this case is shown in Fig. 7(b), and it can be seen that the anomaly is produced by two sources according to this. The minimum norm method and the proposed method are used to invert. The slice at $y = 950$ m of the final inversion result obtained by the minimum norm method and the proposed method is shown in Fig. 7(c) and (d), respectively, and their 3-D perspective views with a truncation density of 0.35 g/cm^3 are shown in Fig. 7(e) and (f), respectively. Notably, it is hard to recover the deep cuboid in this situation with the traditional method, but the performance of the proposed method is highly improved. The deep cuboid has been recovered and accurately located. It is proven that this method is of great significance for deep ore prospecting.

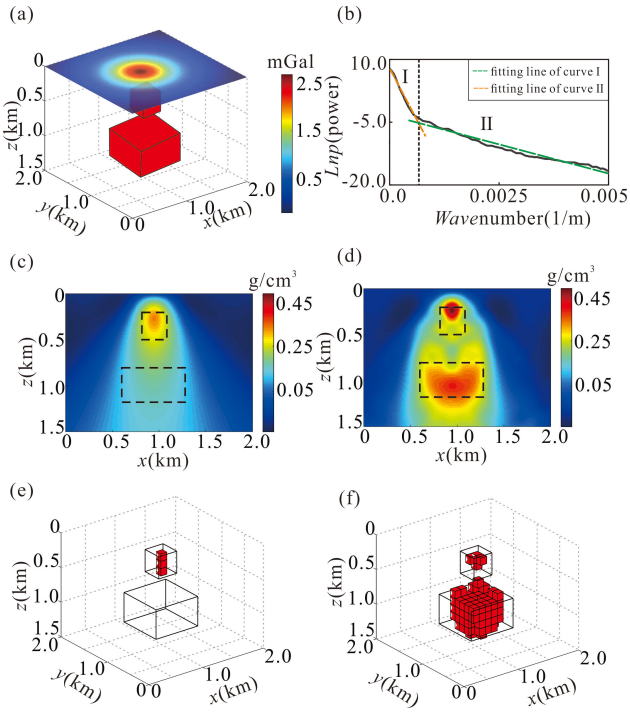

Fig. 7. Two-cuboid-source case in which the central coordinates of the two cuboids are on a vertical line. (a) Cuboid position and its gravity anomaly. (b) Logarithmic power spectrum. (c) Slice at $y = 950$ m of the final inversion result obtained by the minimum norm inversion method. (d) Slice at $y = 950$ m of the combination inversion result obtained by the proposed method. (e) 3-D perspective view of the result by the minimum norm inversion method. (f) 3-D perspective view of the final result by the proposed method.

IV. Field Application

To further verify the applicability in the processing of the actual gravity data, we apply the proposed method to the isostatic gravity anomaly of certain ore-concentrated areas from the west of Zhen'an, South Qinling, China. The mining area is recently discovered in Shaanxi Province in recent years, with superior metallogenic geological conditions. It is located in the inner orogenic belt of the North China plate contiguous with the Qinling orogenic belt in the NE–SW direction. There are two groups of NW-trending and NE-trending tensile–torsional faults in the area. The outcropping strata are mainly Archean and Proterozoic, which are mainly composed of monzonitic granite, quartzite, and argillaceous slate [5]. Magma invades into gneiss along deep faults and accumulates into deposits through crystallization. Due to the change of tectonic background in the region where the deposit is located, the partial melting of the thickened crust leads to magma rising, resulting in strong magmatic activities, which makes the early formed metal deposits undergo different degrees of hydrothermal alteration. Some ore bodies precipitate again to form small-scale ore bodies in favorable areas such as nearby fissures. The gravity data of the ore-concentrated area

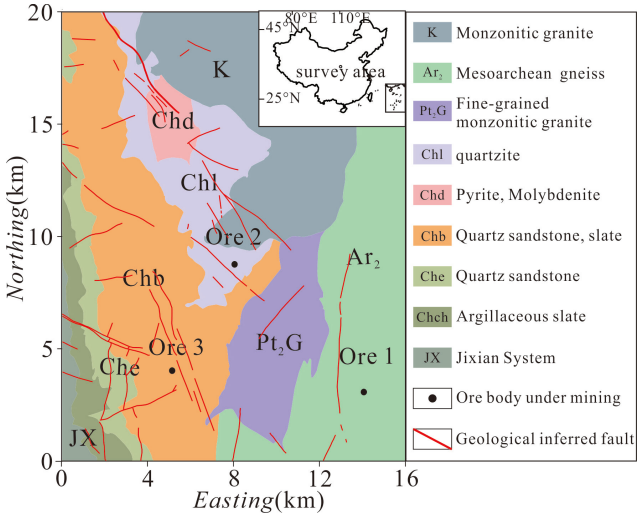

Fig. 8. Geological map of survey area.

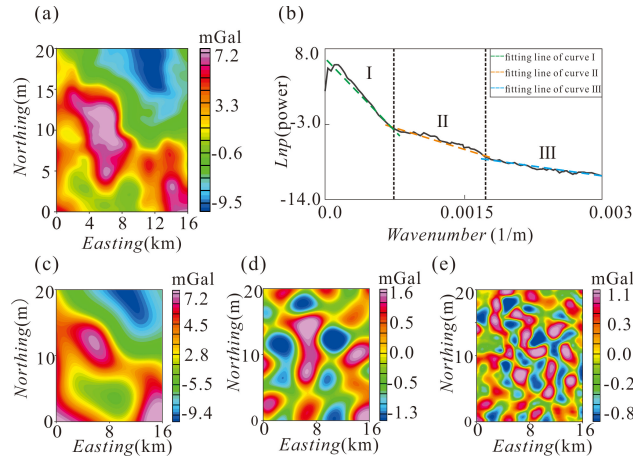

Fig. 9. Isostatic gravity anomaly maps. (a) Isostatic gravity anomaly of survey area. (b) Logarithmic power spectrum. (c) Separated anomaly of I. (d) Separated anomaly of II. (e) Separated anomaly of III.

in Zhen'an were measured by actual field measurements. The scale of the data is 1:20 000 and the precision is ±0.05 mGal. The grid step in the x- and y-directions of field data after gridding is 168 m.

Fig. 8 shows the geological map of the study area obtained according to the geological survey. There are basically three main molybdenum–copper deposits being mined, which are marked Ores 1–3 in the survey area. It can be seen that the ore bodies are mainly developed near the faults. The surrounding rocks are mainly granite and malmstone, and thus, the ore bodies in this area can be regarded as high-density body.

In the isostatic gravity anomaly, which is shown in Fig. 9(a), the ore body is characterized by a high value. According to the slope variation of the radial logarithmic power spectrum in Fig. 9(b), the anomaly is separated into three segments [Fig. 9(c)–(e)] corresponding to different depth information.

The anomalies are inverted by the proposed method with a depth of 6 km to seek the deep potential ore bodies. Since the ore body is characterized by the high-density body, we choose

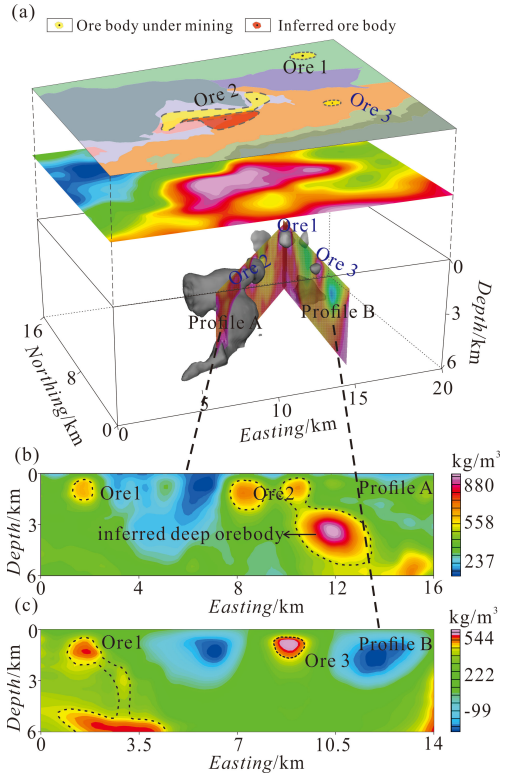

Fig. 10. Combination inversion result of the survey area. (a) 3-D perspective view of the result corresponding to the geological and geophysical map. (b) Slice A. (c) Slice B.

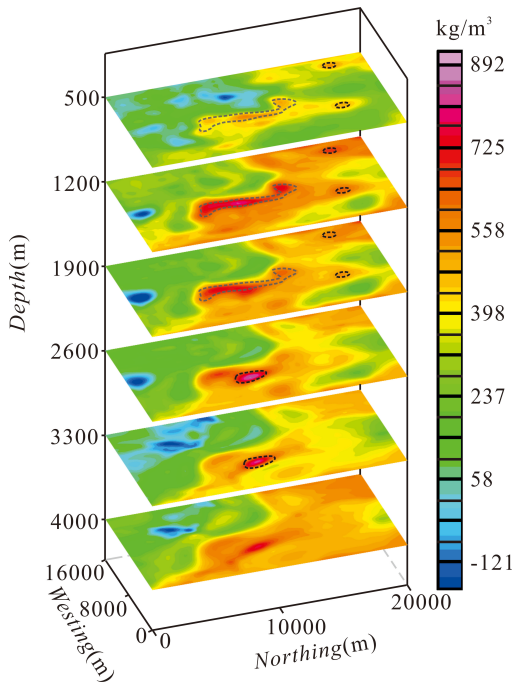

Fig. 11. Horizontal slices of inversion result at different depths.

400 kg/m^3 as the truncation density to show the ore body more clearly. The 3-D perspective view of the inversion result with a 400-kg/m^3 truncation density [Fig. 10(a)] corresponding to the geological map [Fig. 8] and the geophysical map [Fig. 9(a)] is obtained and the slices [Fig. 10(b) and (c)] through three ore body locations are derived from the result.

From Fig 10(a), it is shown that the shallow ore body is recovered well and a high-value body under this ore body in the vertical direction can be distinguished. It can be seen that the positions of the three high-density bodies in the inversion results are in good correspondence with the positions of the exist ore bodies determined in the actual geological survey. In Fig. 10(a), we redraw the scope of the ore body being mined and estimate the possible location of the deep ore body. There is a concealed high-density body below the discovered ore bodies in Profile A. We infer that it may be a potential deep geological body. In Profile B, Ore 1 connects with the high-density body below through the migration channel. We can infer the metallogenic mechanism of ore 1, that is, the ore body above is formed by magma upwelling and migrating through the channel.

To further illustrate the geologically consistent reconstruction ability of the deep source by the proposed method, the horizontal slices of the inversion results at different depths are shown in Fig. 11. In the horizontal slice with depth at 500 m, we can see that the three ore bodies start to show a weak response, and thus, the depth value is supposed to be the top buried depth of ore body. The slice with depth 1200 m shows a stronger response of the bodies and it may pass through the inside of the three bodies. The response gets weak again in the slice with depth at 1900 m; we can infer the buried depth of the three ore bodies according to the slices. In the horizontal slice with depth at 2600 m, a strong response from a deeper block is shown, which is covered by the responses of the shallow ore bodies. According to the horizontal slices, the density changes to further speculate the horizontal range and buried depth of the ore body can be clearly recognized.

V. Conclusion

A 3-D inversion method of gravity anomalies by combining power-spectrum derived adaptive weighting and cross-gradient regularization is developed. According to the model tests, the vertical resolution of the inversion result is relatively improved by adaptive weighting functions to separate anomalies with different burial depths, depending on the logarithmic power spectrum, and the horizontal resolution can also be improved by utilizing the cross gradient to constrain the density structure characteristics of each separated anomaly. Thus, the spatial resolution of the inversion result can be improved relatively by the proposed method. The algorithm of the proposed method is shown effective for the situation where the buried depths of the geological bodies are different. In addition, the method has been validated by the model tests to have stability against Gaussian noise.

This method is also very valuable in practical applications. The proposed method is applied on an ore-concentrated area in Zhen'an and we speculated a high-density body, which could be the potential ore body determined by the inversion result with good quality. It provides a possibility for the conjecture that there are still deep ore bodies in this area. Furthermore, in the absence of other data or prior information, this proposed method could make full use of gravity data to improve the resolution of the inversion results and provide new possibilities for future research exploration. In the next research, the latest drilling data would be added to further constrain the inversion process to verify our existing speculation and obtain more reliable recovered density model.

References

[1] R. M. René, "Gravity inversion using open, reject, and 'shape-of-anomal' fill criteria," *Geophysics*, vol. 51, no. 4, pp. 988–994, Apr. 1986.

[2] M. Fedi and A. Rapolla, "3-D inversion of gravity and magnetic data with depth resolution," *Geophysics*, vol. 64, no. 2, pp. 452–460, Mar. 1999.

[3] F. J. D. Silva, V. C. Barbosa, and J. B. Silva, "3D gravity inversion through an adaptive-learning procedure," *Geophysics*, vol. 74, no. 3, pp. 9–21, Apr. 2009.

[4] J. L. G. Pallero, J. L. Fernández-Martánez, S. Bonvalot, and O. Fudym, "3D gravity inversion and uncertainty assessment of basement relief via particle swarm optimization," *J. Appl. Geophys.*, vol. 139, pp. 338–350, Apr. 2017.

[5] O. Boulanger and M. Chouteau, "Constraints in 3D gravity inversion," *Geophys. Prospecting*, vol. 49, no. 2, pp. 265–280, Dec. 2001.

[6] B. J. Last and K. Kubik, "Compact gravity inversion," *Geophysics*, vol. 48, no. 6, pp. 713–721, Feb. 1983.

[7] A. Guillen and V. Menichetti, "Gravity and magnetic inversion with minimization of a specific functional," *Geophysics*, vol. 49, no. 8, pp. 1354–1360, Aug. 1984.

[8] V. C. F. Barbosa and J. B. C. Silva, "Generalized compact gravity inversion," *Geophysics*, vol. 59, no. 1, pp. 57–68, Jan. 1994.

[9] Y. Li and D. W. Oldenburg, "3D inversion of gravity data," *Geophysics*, vol. 63, no. 1, pp. 109–119, Jan. 1998.

[10] O. Portniaguine and M. S. Zhdanov, "3-D magnetic inversion with data compression and image focusing," *Geophysics*, vol. 67, no. 5, pp. 1532–1541, Oct. 2002.

[11] C. J. Paciorek and M. J. Schervish, "Spatial modelling using a new class of nonstationary covariance functions," *Environmetrics*, vol. 17, no. 5, pp. 483–506, Aug. 2006.

[12] P. Shamsipour, D. Marcotte, M. Chouteau, M. Rivest, and A. Bouchedda, "3D stochastic gravity inversion using nonstationary covariances," *Geophysics*, vol. 78, no. 2, pp. G15–G24, Mar. 2013.

[13] S. Vatankhah, V. E. Ardestani, and R. A. Renaut, "Application of the χ^2 principle and unbiased predictive risk estimator for determining the regularization parameter in 3-D focusing gravity inversion," *Geophys. J. Int.*, vol. 200, no. 1, pp. 265–277, Jan. 2015.

[14] M. H. Ghalehnoee, A. Ansari, and A. Ghorbani, "Improving compact gravity inversion using new weighting functions," *Geophys. J. Int.*, vol. 208, no. 1, pp. 546–560, Jan. 2017.

[15] M. Geng, X. Hu, H. Zhang, and S. Liu, "3D inversion of potential field data using a marginalizing probabilistic method," *Geophysics*, vol. 83, no. 5, pp. G93–G106, Sep. 2018.

[16] Z. Li, C. Yao, and Y. Zheng, "3D inversion of gravity data using L_p-norm sparse optimization," *Chin. J. Geophys.*, vol. 62, no. 10, pp. 3699–3709, Jul. 2019.

[17] V. K. Gupta and N. Ramani, "Some aspects of regional-residual separation of gravity anomalies in a precambrian terrain," *Geophysics*, vol. 45, no. 9, pp. 1412–1426, Sep. 1980.

[18] Y. Li and D. W. Oldenburg, "Separation of regional and residual magnetic field data," *Geophysics*, vol. 63, no. 2, pp. 431–439, Mar. 1998.

[19] G. R. J. Cooper and D. R. Cowan, "Edge enhancement of potential-field data using normalized statistics," *Geophysics*, vol. 73, no. 3, pp. H1–H4, May 2008.

[20] B. K. Bhattacharyya and L. Leu, "Spectral analysis of gravity and magnetic anomalies due to two-dimensional structures," *Geophysics*, vol. 40, no. 6, pp. 993–1013, Dec. 1975.

[21] S. Maus and V. Dimri, "Depth estimation from the scaling power spectrum of potential fields?" *Geophys. J. Int.*, vol. 124, no. 1, pp. 113–120, Jan. 1996.

[22] R. S. Pawlowski and R. O. Hansen, "Gravity anomaly separation by Wiener filtering," *Geophysics*, vol. 55, no. 5, pp. 539–548, May 1990.

[23] A. N. Tikhonov and V. Y. Arsenin, "Solutions of ill-posed problems," *Math. Comput.*, vol. 32, no. 144, p. 491, Apr. 1977.

[24] Y. Li and D. W. Oldenburg, "3-D inversion of magnetic data," *Geophysics*, vol. 61, no. 2, pp. 394–408, Apr. 1996.

[25] B. Cianciara and H. Marcak, "Interpretation of gravity anomalies by means of local power spectra," *Geophys. Prospecting*, vol. 24, no. 2, pp. 273–286, Jun. 1976.

[26] A. Spector and F. S. Grant, "Statistical models for interpreting aeromagnetic data," *Geophysics*, vol. 35, no. 2, pp. 293–302, Apr. 1970.
[27] S. Butterworth, "On the theory of filter amplifiers," *Wireless Eng.*, vol. 7, pp. 536–541, Oct. 1930.
[28] E. Fregoso and L. A. Gallardo, "Cross-gradients joint 3D inversion with applications to gravity and magnetic data," *Geophysics*, vol. 74, no. 4, pp. 31–42, May 2009.
[29] M. Peng, H. D. Tan, and M. Jiang, "Three-dimensional joint inversion of magnetotelluric and seismic travel time data with cross-gradient constraints," *Chin. J. Geophys.*, vol. 56, no. 8, pp. 2728–2738, Jun. 2012.
[30] L. A. Gallardo and M. A. Meju, "Characterization of heterogeneous near-surface materials by joint 2D inversion of DC resistivity and seismic data," *Geophys. Res. Lett.*, vol. 30, no. 13, p. 1658, Jul. 2003.
[31] R. C. Aster, B. Borchers, and C. H. Thurber, "Tikhonov regularization," in *Parameter Estimation and Inverse Problems*, 2nd ed. Boston, MA, USA: Academic, 2013, pp. 93–96.
[32] R. Fletcher and C. M. Reeves, "Function minimization by conjugate gradients," *Comput. J.*, vol. 7, no. 2, pp. 149–154, Jan. 1964.
[33] H. Yan, "Curve smoothing algorithm," in *Principals and Methods of Computer-Aided Cartography*, 2nd ed. Beijing, China: Sci. Press, 2007, pp. 114–116.
[34] L. Ma, X. Qiao, L. Min, B. Fan, and X. Ding, "Shaanxi geological map," in *Geological Atlas of China*, 1st ed. Beijing, China: Geolog. Publishing House, 2002, ch. 8, sec. 6, pp. 318–319.

Guoqing Ma received the B.S. degree in geophysics and the M.S. and Ph.D. degrees in solid geophysics from Jilin University, Changchun, China, in 2008, 2010, and 2013, respectively.

Since 2018, he has been a Professor with Jilin University. From 2017 to 2018, he was a Visiting Scholar with the University of Sydney, Sydney, NSW, Australia. Since 2021, he has been working as the Director of the Department of Geophysics, Jilin University. His research interests are processing and interpretation of multiparameter gravity and magnetic data.

Tingyi Wang received the B.Eng. degree in exploration technology and engineering from Southwest Petroleum University, Chengdu, China, in 2019. She is currently pursuing the M.S. degree in geophysics with Jilin University, Changchun, China.

Her research interests include the study of high-resolution gravity density inversion methods for deep resource exploration, and study of planets' structure and evolution from gravity data.

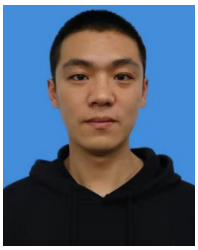

Qingfa Meng received the B.S. degree in geophysics and the M.S. degree in solid geophysics from Jilin University, Changchun, China, in 2016 and 2019, respectively.

His research interests include regularization inversion problem of potential data with different heights and joint inversion of multiple geophysical data.

Zongrui Li received the B.S. and M.S. degrees in geophysics from Jilin University, Changchun, China, in 2018 and 2021, respectively, where he is currently pursuing the Ph.D. degree in geophysics.

His research interest mainly focuses on improving inversion calculation efficiency by using the function fit physical properties distribution method.

Taihan Wang received the B.S. degree in geophysics and the Ph.D. degree in solid geophysics from Jilin University, Changchun, China, in 2013 and 2018, respectively.

From 2018 to 2021, he held a post-doctoral position at Jilin University, where he has been working as an Assistant Professor since 2021. His major research interests include processing, inversion, and interpretation method of gravity, magnetic, and tensor gradient data.

Lili Li received the B.S. degree in geophysics and the M.S. and Ph.D. degrees in solid geophysics from Jilin University, Changchun, China, in 2008, 2010, and 2013, respectively.

Since 2015, she has been an Assistant Professor with Jilin University. Her research interests are processing and interpretation of multiparameter gravity and magnetic data.